

Special relativistic effects in polarised profiles of pulsars

Jarosław Dyks

Nicolaus Copernicus Astronomical Center, Toruń, Poland

Geoffrey A. E. Wright

Astronomy Centre, University of Sussex, Falmer, BN1 9QJ, UK

According to the ‘beads on a wire’ approximation, electrons that flow out of pulsar magnetosphere are dragged into corotational motion by strong magnetic field. We develop a simple analytical model to learn how this phenomenon affects pulse shapes and polarisation. The caustic peaks and fast changes of polarisation angle are found to be intimately related to the regions in pulsar magnetosphere where the curvature of electron trajectories in the inertial observer frame vanishes, or is minimal.

Polarimetry days in Rome: Crab status, theory and prospects

October 16-17, 2008

Rome, Italy

1. Caustic effects

Phase-resolved optical observations of the Crab pulsar (OPTIMA, Słowikowska et al. 2008; HST, Graham-Smith et al. 1996) reveal two interesting polarisation features associated with the maxima in Crab's profile: 1) the minima of polarisation degree and 2) fast changes of polarisation angle (PA).

According to the idea that is recently popular, high-energy profiles of pulsars (including the optical lightcurve of the Crab) are dominated by caustic effects (Morini 1983; Smith 1986; Romani & Yadigaroglu 1995). These caustic effects pile up the radiation emitted on the trailing side of the polar tube within a narrow range of phases. This produces the narrow and strong trailing peaks in gamma-ray pulse profiles. The radiation on the leading side is stretched into the wide, low-level 'bridge' emission.

These caustic effects are usually presented as combined effects of altitude-dependent aberration and retardation (AR), which need to be included when the emission process is considered to occur in the corotating frame (CF). Such a procedure must evidently be flawed, because the standard radiation formulae of classical electrodynamics are not designed for use in a reference frame that is non-inertial with respect to the observer. As soon as we determine the electron motion (trajectory, velocity, acceleration) in the inertial observer frame (IOF) we do not need to be bothered by the aberration anymore. Should we still expect any caustic enhancement on the trailing side? What is its origin, if we have no aberration in IOF?

To answer these questions let us consider the motion of electrons in the plane of rotational equator for a pulsar with orthogonal dipole inclination ($\alpha = 90^\circ$) and viewed at angle $\zeta = 90^\circ$ with respect to the rotation axis $\vec{\Omega}$. Following Dyks, Demorest, Wright, et al. (2009; hereafter DDW), we will first consider the caustic effects in the CF-based approach, and then compare the results with the approach constrained solely to the IOF.

Radiation emitted at a radial distance r from a \vec{B} -field line with footprint parameter s , is detected at the phase:

$$\phi_T \simeq \frac{3}{2}s\sqrt{\frac{r}{R_{lc}}} - 2\frac{r}{R_{lc}} + \phi_f, \quad (1.1)$$

where ϕ_f is the absolute fiducial phase defined in Dyks (2008) and $R_{lc} = cP/2\pi$ is the light-cylinder radius. The square root term simply represents the divergence of dipolar field lines and the linear term represents the AR effects. The positive sign of the square-root term means that the equation refers to the trailing side of the polar flow.

Let the emission be radially extended between $r_1 = r_{av} - \Delta r/2$ and $r_2 = r_{av} + \Delta r/2$, where Δr is the radial extent and r_{av} is the average radial distance of emission. The radiation between r_1 and r_2 is detected within the narrow phase range of:

$$\Delta\phi_T = \phi_T(r_2) - \phi_T(r_1) \simeq \frac{\Delta r}{R_{lc}} \left(\frac{3}{4} \frac{s}{\sqrt{r/R_{lc}}} - 2 \right). \quad (1.2)$$

where we have omitted the index 'av' at r in the denominator and ignored all terms of higher order than $\Delta r/R_{lc}$. The interval of detection phase can thus be squeezed down to a negligible width if the bracket is equal to zero (in which case $\Delta\phi_T \sim (\Delta r/R_{lc})^2$).

In the alternative approach, it is useful first to find the curvature radius ρ_{iof} of electron trajectory in IOF. Assuming that the electron velocity has the fixed value of the speed of light c , the IOF radius of curvature is equal to $\rho_{\text{iof}} = c^2/|\vec{a}_{\text{iof}}|$, where \vec{a}_{iof} is the centripetal acceleration of the electron in the IOF. The acceleration is a sum of two vectors:

$$\vec{a}_{\text{iof}} = \vec{a}_B + \vec{a}_\Omega \simeq \frac{c^2}{\rho_B} \hat{\rho}_B + 2\Omega c \hat{e}_\phi, \quad (1.3)$$

where \vec{a}_B is the CF-acceleration due to the curvature of magnetic lines and \vec{a}_Ω is the acceleration generated by the corotation (see Dyks 2008 for a simple derivation). The symbol ρ_B denotes the radius of curvature of \vec{B} -field lines in the CF: $\rho_B \simeq (4/3)\sqrt{rR_{\text{lc}}}/s$, $\hat{\rho}_B$ (with a hat) is a unit vector along that radius of curvature, and \hat{e}_ϕ is a unit vector in the direction of the rotational azimuth. On the trailing side $\hat{\rho}_B \simeq -\hat{e}_\phi$ so that

$$\rho_{\text{iof}} \simeq R_{\text{lc}} \left| \frac{3}{4} \frac{s}{\sqrt{r/R_{\text{lc}}}} - 2 \right|^{-1}. \quad (1.4)$$

The IOF radius of curvature on the trailing side is increased by the presence of the ‘−2’ term. On the leading side $\hat{\rho}_B \simeq \hat{e}_\phi$ so that ρ_{iof} is given by equation that differs from 1.4 only in the positive sign at the number 2. Hereafter the curvature radii for points located symmetrically on opposite sides of the $(\vec{\Omega}, \vec{\mu})$ plane will be denoted $\rho_{\text{iof,L}}$ and $\rho_{\text{iof,T}}$, where the indices ‘L’ and ‘T’ refer to the leading and trailing side. In the outer parts of the polar region ($s \lesssim 1$) we have $\rho_{\text{iof,L}} < \rho_B < \rho_{\text{iof,T}}$.

With the knowledge of ρ_{iof} the interval of detection phase associated with the radial extent Δr can simply be expressed as:

$$\Delta\phi \simeq \frac{\Delta r}{\rho_{\text{iof}}}, \quad (1.5)$$

which is equivalent to eq. 1.2 obtained within the CF-based approach. Thus *the caustic effects of AR simply correspond to the straightening of trajectories in the IOF*. Fig. 1 illustrates this effect for $\alpha = \zeta = 90^\circ$ and the rotation period of the Crab pulsar.

To answer the question on whether the trailing side is still expected to be brighter (even in this ρ_{iof} -based approach), we note that the more strongly is $\Delta\phi$ squeezed, the larger is the observed flux, so that $F \propto |\Delta\phi|^{-1} \propto \rho_{\text{iof}}$. This confirms the caustic brightening of the trailing side, because ρ_{iof} is larger there than on the leading side. However, the flux asymmetry can be much smaller than the ratio of curvature radii $\rho_{\text{iof,T}}/\rho_{\text{iof,L}}$, because the radiation process can intrinsically depend on ρ_{iof} . For the curvature radiation we have $F_{\text{CR}} \propto \rho_{\text{iof}}^{-2/3}$ (Buschauer & Benford 1980) so that the caustic asymmetry of flux has the magnitude of only $(\rho_{\text{iof,T}}/\rho_{\text{iof,L}})^{-1/3}$. In the case of the curvature radiation the caustic effects are then much weaker than for radiation mechanisms that do not depend on ρ_{iof} .

2. Polarisation

The strongest caustic effects are expected when $\Delta\phi \simeq 0$ which is equivalent to $\rho_{\text{iof}} = \infty$. This happens when the radiation is emitted from locations given by:

$$\frac{r}{R_{\text{lc}}} \simeq \frac{9}{64}s^2, \quad (2.1)$$

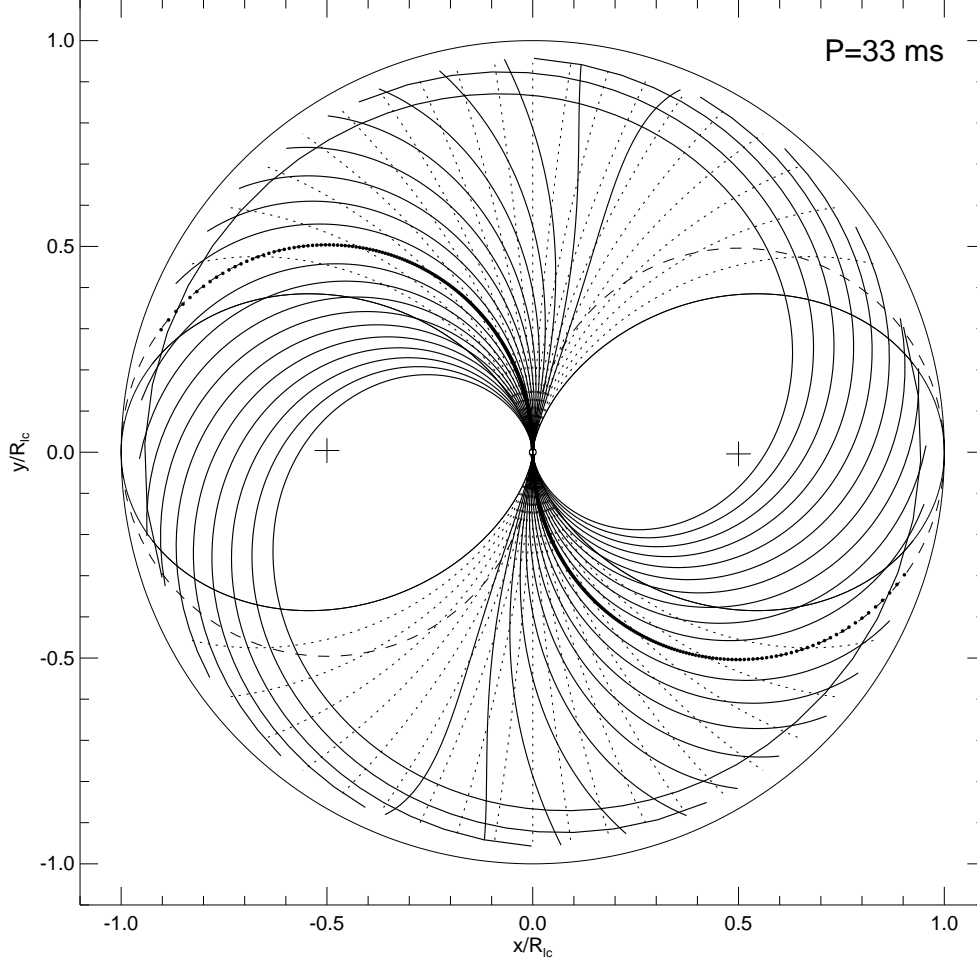


Figure 1: IOF trajectories (thick solid lines) of electrons moving in the equatorial plane of orthogonal pulsar ($\alpha = 90^\circ$). The curves are separated by $\Delta s = 0.1$ and refer to electrons that left the star surface when the dipole axis was vertical in the figure. IOF trajectories for electrons moving along the dipole axis are marked with dots (merging into very thick solid lines) and coincide with the analytical solution (dashed circles of radius $R_{1c}/2$, centered at the crosses on both sides of the star; the centers are located at $x/R_{1c} = \pm 0.5 \mp (0.5R_{NS}/R_{1c})^2$ and $y/R_{1c} = \mp 0.5R_{NS}/R_{1c}$). Electron trajectories in the CF (\vec{B} -field lines) are shown as dotted lines, except from the last open ones, which are thin solid. The outermost circle is the light cylinder. The figure assumes rigid corotation of a static-shape dipole up to $0.95R_{1c}$.

which can be rewritten into

$$\frac{r}{R_{1c}} \simeq \frac{3}{8}\theta, \quad \text{or} \quad \theta \simeq \frac{3}{8}s^2, \quad (2.2)$$

because the footprint parameter $s = \theta/(r/R_{1c})^{1/2}$, where θ is the colatitude measured from the dipole axis. Hereafter the caustic coordinates given by eqs. 2.1 and 2.2 will be denoted r_{cst} , θ_{cst} and s_{cst} .

The caustic peaks are produced when electrons move rectilinearly towards the observer as they pass through the inflection point of their IOF trajectory. At low altitudes ($r < r_{cst}$) the IOF

trajectory is curved in the backward direction (opposite to the direction of local rotation velocity). At large $r > r_{\text{cst}}$ it is bent forward because the corotation dominates over the \vec{B} -field line curvature. At $r = r_{\text{cst}}$ the IOF trajectory has its inflection point.

The equation 2.2 is the same as eq. (3) in Dyks (2008) for the zero-curvature regions associated with the steepest gradient point of the S-curve of polarisation angle. Indeed, according to eq. 1.1, the radiation emitted from the caustic regions (eq. 2.1) is detected at the phase:

$$\phi_{\text{cst}} \equiv \phi_{\text{max}} \simeq \frac{9}{32}s^2 + \phi_f = 2\frac{r}{R_{\text{lc}}} + \phi_f = 16^\circ 11s^2 + \phi_f. \quad (2.3)$$

The equation $\phi_{\text{cst}} \simeq 2r/R_{\text{lc}} + \phi_f$ determines the location of the center of the S-shaped PA curve for a laterally extended emitter ($\Delta s \sim 1$, $\Delta r \sim 0$, Dyks 2008).

Thus we find that both the caustic peaks and the steepest variations of PA in the famous S-swing are associated with the locations of zero (or minimum) curvature of IOF trajectories. However, the S-swing appears for a laterally-extended slab-like emission region, whereas the peaks in high-energy profiles are formed by a radially-extended emitter with a possibly negligible lateral extent ($\Delta s \sim 0$, $\Delta r/R_{\text{lc}} \sim 1$). Moreover, for the Crab pulsar we have $\zeta \simeq 62^\circ$ (Ng & Romani 2004) which is far enough from 90° to complicate analytical considerations.

An interesting question is whether the conclusion that fast PA variations accompany the caustic peaks can be extended to the radially extended case of the slot gap or outer gap model. Numerical simulations (Takata et al. 2007; Dyks et al. 2004, hereafter DHR) tell us that fast changes of PA indeed tend to occur at the peaks, although not always (see eg. figs. 5 and 10 in DHR). A prominent example of such rapid PA swing is the one that occurs at the caustic peak visible at $\phi/360^\circ \simeq 0.12$ in fig. 5 of DHR (panels ‘a’ to ‘e’ with $\zeta < \alpha$). The swing looks ‘similar’ to the one observed in the leading peak of the Crab pulsar by the OPTIMA group. In the following two paragraphs we discuss some aspects of the phenomenon.

When electrons pass through the ‘caustic’ radial distance r_{cst} their acceleration vector becomes rotated from $\hat{\rho}_B$ to \hat{e}_ϕ , because at low altitudes ($r \ll r_{\text{cst}}$) \vec{a}_{iof} is dominated by the curvature of magnetic field lines (first term in eq. 1.3), whereas at large $r \gg r_{\text{cst}}$ the rotational acceleration dominates (second term in eq. 1.3). In the strictly equatorial case ($\alpha = \zeta = 90^\circ$) projections of the vectors $\hat{\rho}_B$ and \hat{e}_ϕ on the plane of the sky maintain exactly opposite directions so that at $r = r_{\text{cst}}$ the PA jumps discontinuously by 180° which can leave no trace in the data. However, a continuous change of PA is expected in a non-planar case. The fast variations of PA at caustic peaks might therefore seem likely even for the radially extended emitters. The problem is that in the simplest-case situation (small angle approximation, strictly orthogonal geometry), the radiation emitted *both* at $r < r_{\text{cst}}$ and $r > r_{\text{cst}}$ is detected at $\phi < \phi_{\text{cst}}$. The phase ϕ_{cst} is the ‘maximum possible’ detection phase for a \vec{B} -field line with a given s (to see this clearly it is useful to draw/imagine/consider tangents to an S-shaped IOF trajectory in the vicinity of its inflection point). At $\phi \lesssim \phi_{\text{cst}}$ the radiation emitted at two different altitudes is observed simultaneously. When the line of sight passes through the caustic peak the behaviour of PA becomes irrelevant because the flux sharply drops down to zero as soon as the peak’s maximum is observed.

In the specific (and a bit more realistic) case of the numerical calculation ($90^\circ \neq \alpha \neq \zeta \neq 90^\circ$, $s = 1$) the situation is qualitatively different. When our line of sight passes through the caustic peak, it samples radiation originating from magnetic field lines with different magnetic azimuth ϕ_m

(measured around the magnetic axis) as well as from different r . The radial distance of emission changes very fast with ϕ : during the passage through the sweep the observed r changes from $\sim 0.2R_{lc}$ to $\sim 0.6R_{lc}$ (see fig. 13 in DHR). The observer detects radiation from a given \vec{B} -field line at two different phases. For the first time it happens before the rapid swing begins (low altitudes are seen, $r < r_{cst}$). For the second time the same line is seen within or after the swing (but now we see radiation from larger altitudes). The situation is therefore more complicated than in the degenerate uni-planar case that we were able to study analytically. However, the fast transition from the low to high altitudes again suggests the passage from the \vec{B} -field dominated to the rotationally dominated acceleration (in the non-planar geometry $\hat{\rho}_B$ and \hat{e}_ϕ in eq. 1.3 have different directions).

Although our model is of only linear order in r/R_{lc} , the equations 2.3 and 1.4 trace quite well the locations of the caustic phase and infinite curvature, as we verified numerically. The agreement is of the order of 1% for normal (slow) pulsars and $\sim 10\%$ for fast millisecond pulsars. Because of the approximate character of the analytical model, one can neglect the influence of general relativistic effects on the ray propagation and time delays. The initial (low-altitude) directions of ray propagation are close to radial, which makes the gravitational bending inefficient. Large altitude differences ($\Delta r \sim R_{lc}$) can introduce measurable Shapiro delay (a few degrees of phase) only for fast millisecond pulsars ($P \lesssim 3$ ms). For $P \sim 1$ s the delays are as small as a few hundredths of a degree. See eg. Braje, Romani & Rauch (2000), or Gonthier & Harding (1994) for a closer study of general relativistic effects.

Acknowledgments

The work was supported by the grant N203 017 31/2872 of the Ministry of Science and Higher Education. GAEW thanks the University of Sussex for a Visiting Research Fellowship.

References

- [1] Braje, T.M., Romani, R.W., & Rauch, K.P. 2000, ApJ, 531, 44
- [2] Buschauer R., & Benford G., 1980, MNRAS, 190, 945
- [3] Dyks J., 2008, MNRAS, 391, 859
- [4] Dyks J., Demorest P., Wright G.A.E., et al., 2009, MNRAS, submitted (DDW)
- [5] Dyks J., Harding A. K., & Rudak B., 2004, ApJ 606, 1125 (DHR)
- [6] Gonthier, P.L., & Harding, A.K. 1994, ApJ, 425, 767
- [7] Graham-Smith F., Dolan J.F., Boyd P.T., et al. 1996, MNRAS, 282, 1354
- [8] Morini M., 1983, MNRAS, 202, 495
- [9] Ng C.-Y., & Romani R.W., 2004, ApJ, 601, 479
- [10] Romani R.W., & Yadigaroglu I.-A., 1995, ApJ, 438, 314
- [11] Słowińska A., Kanbach G., Kramer M., & Stefanescu A., 2008, AIP Conf. Proc., 984, 51
- [12] Smith F. G., 1986, MNRAS, 219, 729
- [13] Takata J., Chang H.-K., & Cheng K.S., 2007, ApJ, 656